Mon. Not. R. Astron. Soc. **000**, 1–16 (2002) Printed 23 November 2010 (MN LATEX style file v2.2)

Chemical abundances in the protoplanetary disk LV 2 (Orion): clues to the causes of the abundance anomaly in H II regions

Y. G. Tsamis[1,2,3⋆], J. R. Walsh[2], J. M. Vílchez[1], and D. Péquignot[4]†
[1] *Instituto de Astrofísica de Andalucía (CSIC), Apartado 3004, 18080 Granada, Spain*
[2] *European Southern Observatory, Karl-Schwarzschild-Str. 2, D-85748 Garching bei München, Germany*
[3] *Department of Physics and Astronomy, The Open University, Walton Hall, Milton Keynes MK7 6AA*
[4] *LUTH, Observatoire de Paris, CNRS, Université Paris Diderot, 5 Place Jules Janssen, 92190 Meudon, France*

arXiv:1009.4783v2 [astro-ph.GA] 21 Nov 2010

Accepted XXX December XX. Received XXX December XX; in original form XXX October XX

ABSTRACT

Optical integral field spectroscopy of the archetype protoplanetary disk LV 2 in the Orion Nebula is presented, taken with the VLT FLAMES/Argus fibre array. The detection of recombination lines of C II and O II from this class of objects is reported, and the lines are utilized as abundance diagnostics. The study is complemented with the analysis of *HST* Faint Object Spectrograph ultraviolet and optical spectra of the target contained within the Argus field of view. By subtracting the local nebula background the intrinsic spectrum of the proplyd is obtained and its elemental composition is derived for the first time. The proplyd is found to be overabundant in carbon, oxygen and neon compared to the Orion Nebula and the sun.

The simultaneous coverage over LV 2 of the C III] λ1908 and [O III] λ5007 collisionally excited lines (CELs) and C II and O II recombination lines (RLs) has enabled us to measure the abundances of C^{2+} and O^{2+} for LV 2 with both sets of lines. The two methods yield consistent results for the intrinsic proplyd spectrum, but not for the proplyd spectrum contaminated by the generic nebula spectrum, thus providing one example where the long-standing abundance anomaly plaguing metallicity studies of H II regions has been resolved. These results would indicate that the standard forbidden-line methods used in the derivation of light metal abundances in H II regions in our own and other galaxies underestimate the true gas metallicity.

Key words: ISM – abundances; HII regions; ISM: individual objects – (LV2, 167-317, Orion Nebula); stars: pre-main-sequence; protostars; planets and satellites: protoplanetary disks

1 INTRODUCTION

LV 2 (167-317; O'Dell & Wen 1994) is found within the area defined by the stars of the Trapezium cluster in the Orion Nebula (M42). Its first characterization was made by Laques & Vidal (1979) who imaged it as an unresolved 'nebular condensation' in the Hα, Hβ and [O III] λ5007 emission lines and proposed that it is a partially ionized high-density globule, a class apart from Bok globules or Herbig-Haro objects. Its true form along with many similar objects, that of a *protoplanetary disk* or 'proplyd', was revealed later in *HST* images (O'Dell et al. 1993; O'Dell & Wen 1994). The currently accepted model for the proplyds is that they are semi-ionized globules harbouring a pre-main sequence star girdled by an accreting, and possibly planet-forming, disk (McCaughrean & O'Dell 1996; Johnstone et al. 1998; Bally et al. 2000). While molecular material photoevaporated from the disk is shielded from ionizing Lyman continuum radiation, proplyds that are situated within the main H II region are being exposed to both direct (stellar) and diffuse (scattered in the nebula) ionizing photons with energies greater than 13.6 eV and they become radiation-bounded, surrounded by an ionization front.

Fig 1 shows an *HST* image of LV 2 in the light of Hα

⋆ E-mail: ytsamis@eso.org
† Based on observations made with ESO telescopes at the Paranal Observatory (078.C-0247(A); PI: Tsamis) and on observations made with the NASA/ESA Hubble Space Telescope (PID 6034; PI: Walsh).

© 2002 RAS

(O'Dell & Wen 1994); its main features are the brightest portion of the ionization front ('cusp') facing in the direction of θ^1 Ori C – the main ionizing source in M42 – and an outflow trailing in the opposite direction. The proplyd also possesses a bipolar jet whose brightest lobe is visible on Fig. 1 (Meaburn et al. 1993; Henney et al. 2002; Doi et al. 2004). A number of known properties of LV 2 are summarized by O'Dell et al. (2008). A previous integral field spectroscopic study of LV 2 was presented by Vasconcelos et al. (2005) who observed the 5515 – 7630 Å range with Gemini GMOS focusing on the morphology and kinematics.

In this work we examine the physical properties of LV 2 and those of its immediate M42 vicinity via VLT optical integral field spectroscopy and *HST* Faint Object Spectrograph UV and optical spectra placing emphasis on the elemental composition of the proplyd. LV 2 is in effect used as a probe of the extinction, density, temperature, and chemical abundance structure of the Orion Nebula at subarcsecond (milliparsec) scales. Previous works have found no evidence for substantial electron temperature ($T_{\rm e}$) variations in M42 in the plane of the sky (Rubin et al. 2003), but larger variations across the volume of the nebula have been posited (O'Dell et al. 2003). The proplyds themselves represent localized density enhancements reaching electron densities ($N_{\rm e}$) of $\sim 10^6$ cm^{-3} (Laques & Vidal 1979; Henney et al. 2002) and most of them are embedded in the diffuse H II region ($N_{\rm e}$ $\sim 10^3$–10^4 cm^{-3}; Esteban et al. 2004). Along lines of sight crossing proplyds the reliability of classic temperature diagnostic ratios ([O III] λ4363/λ5007, [N II] λ5754/λ6584) is compromised: spuriously high values of $T_{\rm e}$ are derived when their inherently high densities are overlooked (Walsh & Rosa 1999; Rubin et al. 2003; O'Dell et al. 2003; Mesa-Delgado et al. 2008; Tsamis et al. 2009).

Importantly, it is currently unknown what the abundances of elements in proplyds are and whether they are different from those of the well-studied background nebula or of the main sequence stars in Orion. The chemical composition of planet-forming circumstellar envelopes is of great current interest given the established positive correlation between host star metallicity and the incidence of giant planetary companions (e.g. Gonzalez 1997; Santos, Israelian & Mayor 2000; Gonzalez et al. 2001; Laws et al. 2003; Neves et al. 2009).

Of equal importance is to examine what, if any, the role of proplyds might be in the context of the long-standing abundance anomaly affecting studies of galactic and extragalactic H II regions, whereby larger abundances are derived from the optical recombination lines (RLs) than from the collisionally excited lines (CELs) of oxygen and carbon ions (e.g. Peimbert et al 1993; Tsamis et al. 2003a; Peimbert 2003; Esteban et al. 2004; García-Rojas et al. 2004; Tsamis & Péquignot 2005; Ercolano 2009; Esteban et al 2009; Mesa-Delgado et al 2008, 2010). Here the first detailed study of a proplyd geared towards tackling these open issues is presented.

2 OBSERVATIONS AND REDUCTIONS

Integral field spectroscopy of LV2 was performed on the 8.2-m VLT/UT2 Kueyen during period 78 with the FLAMES Giraffe Argus array. A description of the instrument can be

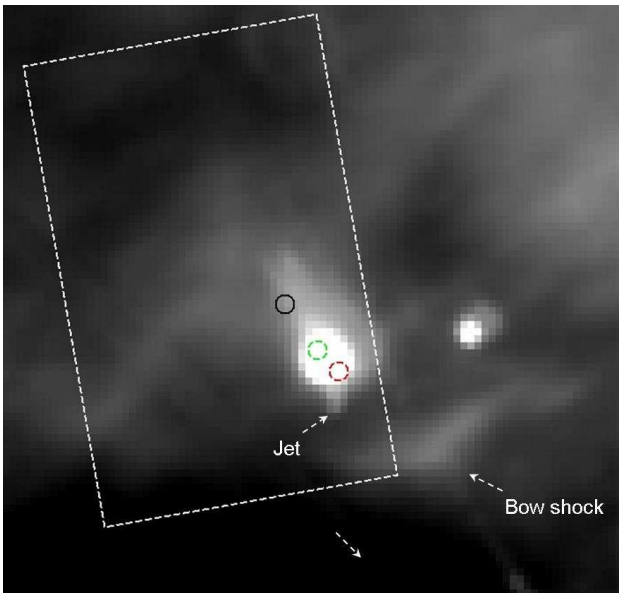

Figure 1. The object near the centre of this *HST* WFPC2 Hα + [N II] image (F656N filter) is the proplyd LV 2 (167-317) at a scale of 0.0996″ pixel^{-1}. The overlaid rectangle is the 6.6″ × 4.2″ field of view of the VLT Argus fibre array. The circles denote the 0.26″ diameter *HST* FOS apertures corresponding to the 'tip' (red), 'core' (green), and 'tail' (black) positions discussed in the text. The arrow towards the bottom right points in the direction of the ionizing source θ^1 Ori C. A diffraction spike from θ^1 Ori C that was extending within the Argus field of view was removed using interpolation from neighbouring pixels. The proplyd outside the Argus field of view is 166-316. North is up and east is to the left.

Table 1. Journal of observations.

Date (UT)	λ-range (Å)	Grating	Exp. time (sec)
		VLT FLAMES[a]	
2006/10/09	3062–4081	LR1	2×150
”	3964–4567	LR2	3×390
”	4501–5078	LR3	4×206
2006/10/07	5015–5831	LR4	3×255
”	5741–6524	LR5	3×255
”	6438–7184	LR6	3×180
		HST FOS[b]	
1996/02/17	1590–2312	G190H	200,200,100,70,30
”	2222–3277	G270H	90,58,80,40,60
”	3235–4781	G400H	440,666,220,200,230
”	4569–6818	G570H	880,1080,200,200,190
”	6270–8500	G780H	100,120,80,60,100

[a] The Argus array was centered at (RA, Dec)$_{\rm JD2000}$ = ($05^h35^m16.857^s$, $-05°23'15.03''$) at a position angle of −80 deg.

[b] The exposure times per grating sequentially refer to the following coordinates (RA, Dec)$_{\rm JD2000}$: M42 filament ($05^h35^m16.119^s\pm0.06''$, $-05°24'09.82''\pm0.07''$); M42 background ($05^h35^m16.220^s\pm0.06''$, $-05°24'09.47''\pm0.07''$); LV 2 tip ($05^h35^m16.737^s\pm0.135''$, $-05°23'16.48''\pm0.07''$); LV 2 core ($05^h35^m16.757^s\pm0.045''$, $-05°23'16.17''\pm0.07''$); LV 2 tail ($05^h35^m16.787^s\pm0.03''$, $-05°23'15.52''\pm0.07''$).

found in Pasquini et al. (2002). A field of view of 6.6 × 4.2 arcsec^2 was used yielding 297 positional spectra in the 3062 – 7184 Å range from six partially overlapping grating settings. The size of the spatial resolution element was 0.31 × 0.31 arcsec^2, corresponding to 123 × 123 AU^2 at the distance to M 42 (412 pc; Reid et al 2009). The location of the Argus field on the Trapezium region of M42 is shown in Fig. 1. The Argus data were reduced with the girBLDRS pipeline developed by the Geneva Observatory which includes the cosmic-ray removal, the flat-fielding, and the wavelength calibration via Th-Ar lamp exposures (Blecha & Simond 2004). The flux calibration was done within IRAF using contemporaneous exposures of various spectrophotometric standards for the grating settings [EG 21 (LR1), Feige 110 (LR2, LR3), LTT 7987 (LR4–6)]. Custom-made scripts were used to construct data cubes and spectral line maps, and a χ^2 minimization routine was used to fit Gaussians to the emission lines (cf. Tsamis et al. 2008).

The observed data cubes are subject to atmospheric refraction as a function of wavelength, known as differential atmospheric refraction (DAR). The direction of DAR is along the parallactic angle at which the observation is made. The six wavelength- and flux-calibrated data cubes for Giraffe low resolution modes LR1 to LR6 were corrected for this effect using the algorithm outlined by Walsh & Roy (1990); using the airmass information this procedure calculates fractional pixel shifts for each monochromatic slice of a cube relative to a fiducial wavelength (e.g. a strong emission line), shifts each slice with respect to the orientation of the slit on the sky and the parallactic angle and recombines the DAR-corrected data cube. The wavelength overlap of each LR setting does not always allow a strong (e.g. H I or He I) line to be used to align each data cube to correct for pointing differences between different grating set-ups. The LV 2 proplyd was the only compact feature that could be used to align the images across the Argus field. The LR1, LR2, LR3 and LR6 cubes were aligned using, respectively, the Hϵ, Hγ, Hβ and Hα lines; the LR5 cube was aligned using He I λ5876 by comparison with He I λ4471 from the LR2 cube. For the LR4 range (5015–5830 Å), a sum of the prominent (forbidden) lines – [N I], [Cl III] and [N II] – was used to compare with Hβ to determine the shift. The shifts required to align all the cubes were generally about 0.25 spaxels (0.08″) except for the LR1 cube whose shift was larger (0.20″). A result of this process is that the corrected maps are no longer of identical extent, depending on the shifts applied, but are suitable for line ratio maps to be constructed that have fidelity on a spaxel-to-spaxel basis over their common imaged area.

LV 2 and its surroundings were also observed with the *HST* Faint Object Spectrograph (FOS) in 1996 in programme 6034. The FOS Red detector (mode FOS/RD) was employed with five gratings giving a total coverage from 1590 to 8500 Å with overlap between each spectral range (Keyes et al. 1995). The 0.3 arcsec single circular aperture was used which projects to 0.26 arcsec on the sky in the aberrated *HST* beam. Five positions on and in the near vicinity of LV 2 were observed. The positions were established by relative astrometry on an *HST* WFPC2 Hα + [N II] image taken in programme 5085 (PI: C. R. O'Dell). Offsets were then specified from a star at $05^h35^m17^s.0, -05°23'34''.3$ of 15th mag. (in the V band) selected from the catalogue of Orion stars by Jones & Walker (1988). This star was centred in the FOS aperture with a series of acquisition peak-ups in successively smaller apertures down to the observing aperture and then the offsets, measured from this star to the observing positions on the WFPC2 image, were applied.

Three positions around LV 2 were observed: the peak of LV2 (called 'Core'), 0.6 arcsec southwest of the peak (called 'Tip') and 1.0 arcsec northeast of the peak (called 'Tail'); see Fig. 1 for these aperture positions which are contained within the Argus field of view. In addition two further positions, on an [S II]-bright filamentary 'ridge' of emission ('M42-filament') and a background position 1.5 arcsec east of this filament ('M42-background'), were observed; these fall outside the Argus field of view ∼55 arcsec southwest from its centre. Table 1 lists the respective exposure times of all the grating settings and positions. The standard pipeline reduction products were used for the FOS data and emission line fluxes were determined by fitting Gaussians to the extracted 1D flux and error spectra.

3 ANALYSIS OF *HST* FOS DATA

The FOS spectra were used for the computation of the physical conditions and abundances of the targeted positions, and as a means to independently check the reliability of the FLAMES spectrophotometry for the overlapping LV 2 positions. Spectra of the LV 2 core and tail observations are shown in Fig. 2. In Table 2 we present the dereddened fluxes for the strongest lines detected at each position, along with the electron densities and temperatures derived from standard diagnostic line ratios.[1] The adopted logarithmic reddening coefficient, c(Hβ), was obtained from the Hα/Hβ, Hγ/Hβ and Hδ/Hβ flux ratios using the modified Cardelli, Clayton & Mathis (1989; CCM) law from Blagrave et al. (2007) with a total to selective extinction ratio $R_V = 5.5$ applicable to M42. Values of c(Hβ) were also deduced from a comparison of the observed [O II] λ2470/λ7320+30 line ratio to the almost invariant theoretical value of 0.75 taken from Zeippen (1982) (Table 2). These measurements typically suffer from larger uncertainties than the Balmer decrement. It is also possible that stellar light scattered within the nebula selectively enhances the UV/blue lines (e.g. O'Dell & Harris 2010) leading to lower reddening deduced from the UV/red [O II] ratio for the M42 filament and background positions than from the Balmer decrement; in view of this the c(Hβ) values from [O II] were not used in this analysis.

Electron densities were derived from the [S II] λ6731/λ6716 doublet ratio and the [O II] λ3726/λ2470 ratio. The former diagnostic is not sensitive to densities $\gtrsim 10^4$ cm^{-3}, while the latter is sensitive up to a few times 10^6 cm^{-3} (e.g. Osterbrock 1989). At the same time the [O II] ratio is somewhat T_e-sensitive: typically, higher [O II] densities are returned for lower temperatures. The temperature applicable to the O^{2+} zone was derived from the [O III] λ5007/λ4363 ratio. For each FOS position the mean T_e([O III]) is quoted in Table 2 with a range corresponding to an adopted upper and lower density boundary. Those boundaries were taken

[1] These were computed using the code EQUIB developed at University College London.

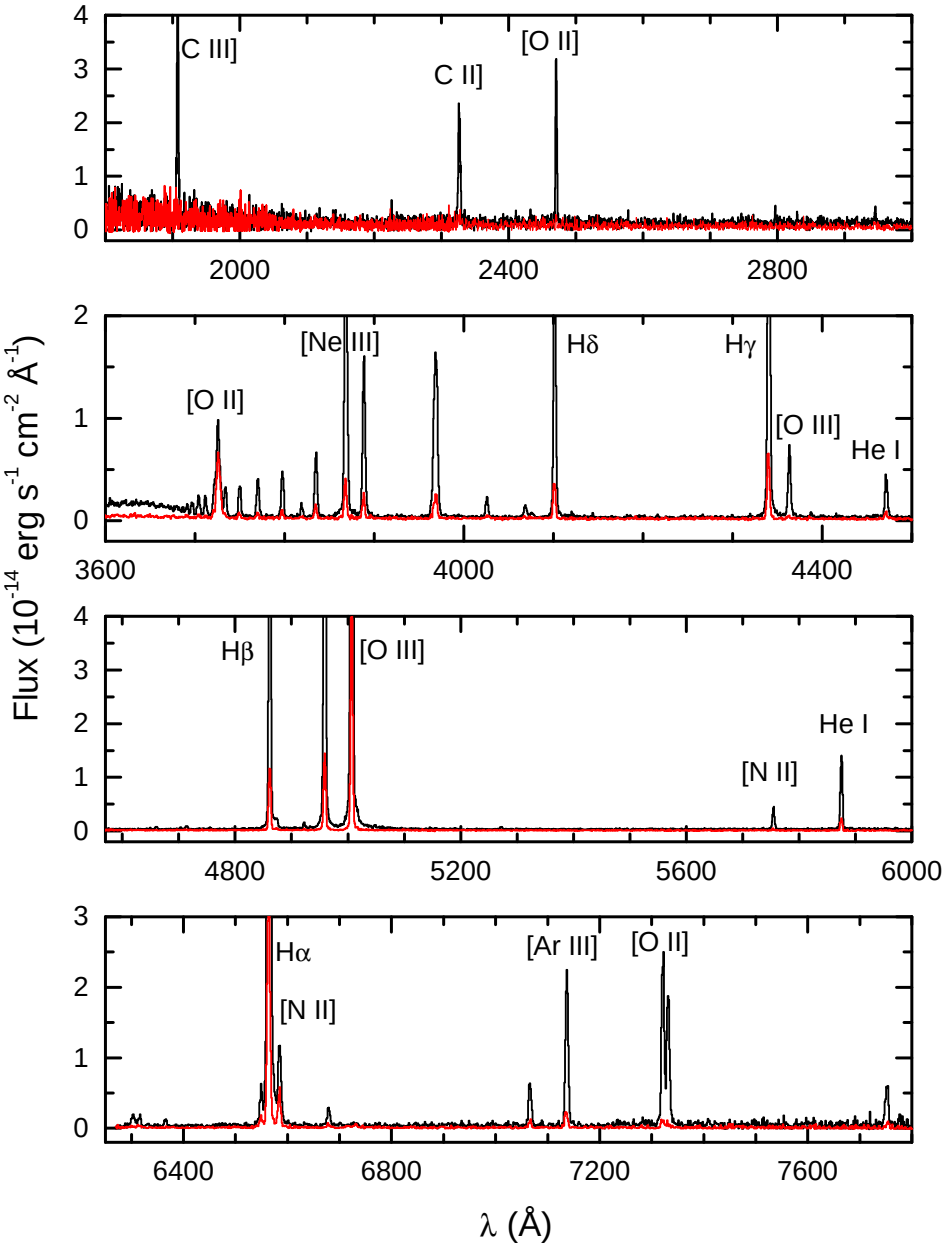

Figure 2. *HST* FOS spectra of LV 2 core (black) and tail (red) positions as defined in Fig. 1 (not corrected for reddening).

from the positions where the [O II] and [N II] curves cross the [O III] curve on the (T_e, N_e) diagnostic plane for the M42 filament, and LV 2 tip and tail positions. The [N II] $\lambda5754/\lambda6584$ ratio, just like the [O II] $\lambda3726/\lambda2470$ ratio, is mostly density sensitive for these positions. For LV 2 core the upper density boundary was taken to be 10^6 cm^{-3} (see Section 4.2). The auroral [N II] $\lambda5754$ and [O III] $\lambda4363$ lines are not detected in the M42 background spectrum and hence no T_e is available for it.

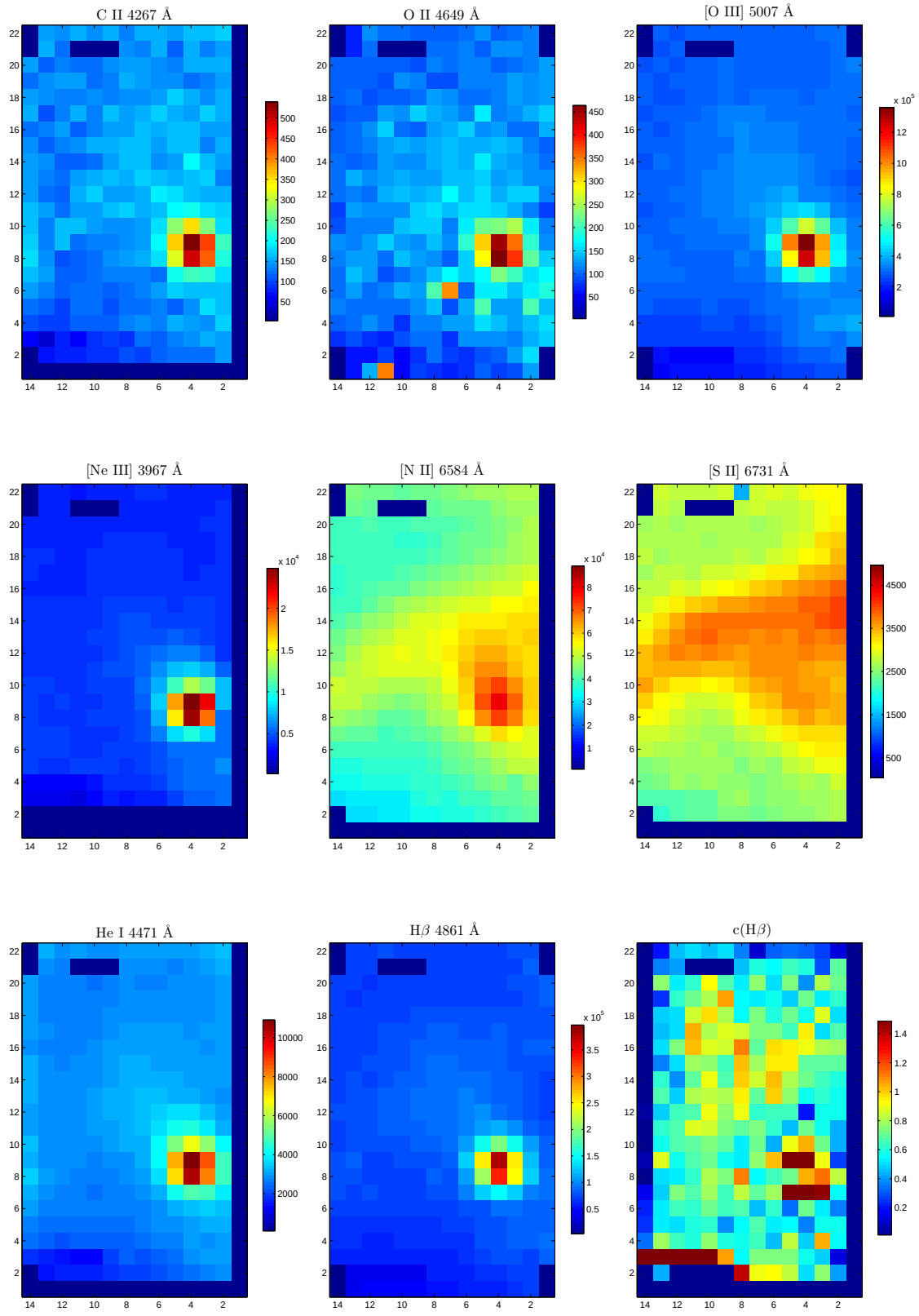

Figure 3. Monochromatic observed flux maps in emission lines arising from LV 2 and vicinity (in units of 10^{-18} erg s^{-1} cm^{-2} per spaxel). Recorded with the 6.6″ × 4.2″ VLT Argus fibre array with 0.31″×0.31″ spaxels (from top to bottom and left to right): C II λ4267, O II λ4649, [O III] λ5007, [Ne III] λ3967, [N II] λ6584, [S II] λ6731, He I λ4471, Hβ λ4861, and the reddening constant from the Hγ/Hβ ratio [the spaxels which show up with large values on row 3 of the c(Hβ) map have been excluded from any analysis]. Spaxels (9–11, 21) correspond to broken fibres. Dark blue masked out rows/columns are artifacts at the edges of the array introduced during the correction for differential atmospheric refraction (2 spaxels per corner are blank by default as they correspond to sky fibres).

Table 2. Line fluxes and physical conditions of M42 and LV 2 positions from *HST* FOS data.[a]

	M42 filament	M42 background	LV 2 tip	LV 2 core	LV 2 tail	LV 2 core − tail
c(Hβ)	0.77±0.07	0.71±0.07	0.59±0.07	0.72±0.02	0.68±0.06	0.70±0.02
c(Hβ)	$0.46^{+0.16}_{-0.14}$	$0.49^{+0.45}_{-0.27}$	$1.01^{+0.14}_{-0.12}$	$0.65^{+0.09}_{-0.12}$	$0.78^{+0.62}_{-0.31}$	0.70±0.07
F(Hβ)	0.385±0.02	0.340±0.02	1.10±0.02	3.53±0.04	0.539±0.02	2.99±0.04
I(C III] λ1908)	16.0±5.5	13.1±8.7	42.4±7.2	75.2±5.8	–	87.4±7.0
I(C II] λ2326)	46.8±8.0	13.1±8.5	21.5±3.8	47.6±4.3	$\lesssim$0.510	55.2±6.1
I([O II] λ2470)	24.8±4.4	12.4±4.8	15.7±2.3	34.9±2.5	7.10±3.80	39.4±3.8
I([O II] λ3726+29)	171±5	143±6	34.2±1.6	17.2±0.4	75.9±3.1	8.92±0.86
I([Ne III] λ3869)	12.7±1.3	13.7±2.0	43.8±1.6	45.3±0.9	30.6±1.8	47.6±2.1
I(He I λ4471)	3.70±0.8	3.65±1.13	4.69±0.59	4.47±0.30	4.34±0.89	4.49±0.39
I([O III] λ4959)	68.4±3.6	99.5±4.8	144±3	133±1	121±3	135±2
I(He I λ5876)	10.7±1.7	12.1±2.1	13.7±0.95	14.0±0.5	13.5±1.2	14.1±0.6
I([S III] λ6312)	1.07±0.04	–	1.47±0.40	1.96±0.25	3.18±1.69	2.00±0.35
I([N II] λ6584)	104±7	60.0±6.8	18.3±1.4	18.3±0.8	41.6±3.8	14.5±1.0
I(He I λ6678)	3.22±1.6	2.18±1.04	3.29±0.67	4.06±0.39	3.64±1.48	4.13±0.45
I([S II] λ6731)	12.3±2.6	2.06±0.08	1.55±0.44	0.512±0.193	4.13±1.52	–
I([Ar III] λ7135)	8.73±2.9	14.5±3.0	41.4±1.9	24.1±1.5	15.6±2.2	25.5±1.9
I([O II] λ7320+30)	25.6±5.4	13.5±4.1	40.8±5.9	46.6±2.5	11.2±0.7	52.3±5.5
[O III] λ4959/λ4363	63.9±6.3	–	27.6 ±3.0	17.4±0.9	63.5±21.4	15.7±0.9
[N II] λ6584/λ5755	31.3±8.6	–	12.7±1.7	4.22±0.21	28.2±11.2	3.03±0.32
[S II] λ6731/λ6716	2.53±1.06	1.75±0.26	3.73±1.68	–	1.78±1.54	–
N_e [S II] (cm^{-3})	>2300	4300^{+5500}_{-2100}	$\gtrsim 10^4$	–	4800:	–
N_e [O II] (cm^{-3})[b]	$1.7^{+0.4}_{-0.2}\times10^4$	$1.1^{+0.8}_{-0.4}\times10^4$	$4.5^{+0.7}_{-0.4}\times10^4$	$2.0^{+4.2}_{-0.3}\times10^5$	$1.0^{+0.9}_{-0.3}\times10^4$	$6.6^{+0.1}_{-0.1}\times10^5$
N_e [N II] (cm^{-3})	$6.5^{+2.2}_{-1.9}\times10^4$	–	$1.4^{+0.14}_{-0.9}\times10^5$	$5.7^{+0.2}_{-3.8}\times10^5$	$7.9^{+7.1}_{-6.2}\times10^4$	$1.0^{+0.1}_{-0.3}\times10^6$
T_e [O III] (K)	8850±250	–	10950±550	10700±1300	8950^{+1550}_{-1250}	9050±650

[a] c(Hβ) in row 1 were deduced from the H I Balmer ratios, in row 2 from the [O II] λ2470/λ7320+30 ratio. The former were adopted; F(Hβ)'s correspond to observed fluxes within a 0.26″ diameter aperture (in units of $\times10^{-13}$ erg cm^{-2} s^{-1}); $I(\lambda)$ denotes dereddened intensities in units of Hβ = 100;

[b] Derived from the $I(\lambda3726)/I(\lambda2470)$ ratio for $T_e = T_e$([O III]); for 'M42 background' 8400 K was adopted from the Argus background spectrum.

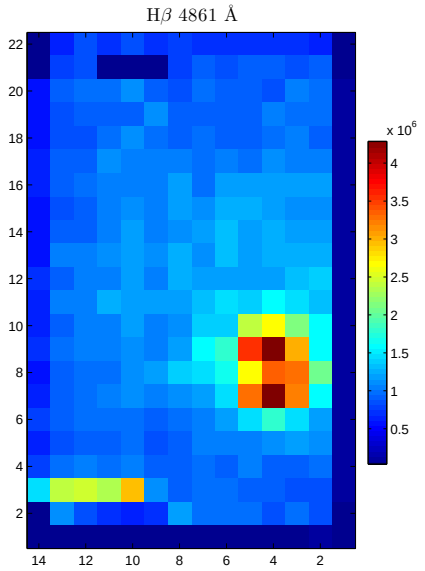

Figure 4. A dereddened Hβ image of LV 2 computed using the extinction map of Fig. 3 (in units of 10^{-18} erg s^{-1} cm^{-2} per spaxel).

4 ANALYSIS OF VLT ARGUS DATA

The FLAMES Argus data were used in two ways: to create spectral maps of LV 2 and its vicinity, and to obtain summed spectra for various regions. The (X=14, Y=22, λ) spectral cube was co-added spatially over spaxels (3–5, 7–10), (4–9, 11–15), and (4–11, 18–20) + (7–12, 4–5) + (11–12, 6–17) to yield one-dimensional spectra for three regions respectively encompassing the core, tail and local background of LV 2 (X and Y are respectively measured on the minor and major axis of the Argus array). These regional spectra were scaled to the same number of spaxels and then the background spectrum was subtracted from the other two so that pure proplyd spectra were obtained. The subtraction resulted in spectra of LV 2 that are free from both nebular (M42) and telluric emission; these will be hereafter called the Core and Tail spectra. To orientate the discussion, maps of LV 2 in several emission lines including Hβ are shown in Fig 3. These show the observed field without any background subtraction.

The proplyd is marginally resolved in the emission line maps, with a FWHM of about 2.5 spaxels (0.78 arcsec). There is no conclusive evidence of this varying between H I and He I, O II, C II, [O III] or [Ne III]. However at the longer wavelengths in the low ionization lines [N II] λ6584 and [S II] λ6731 the contrast of LV 2 against the background is low and the FWHM may be larger. In these lines there is a strong ionization front feature extending across the field of view

from NW to SE (seen also in Fig. 1); this could arise in the nebula background but could also partially be intrinsic emission from the tail itself. The form of the tail does not differ noticeably between Hβ, He I, [O III] or [Ne III] presenting a fan shape (as it does on the *HST* image of Fig. 1). The signal-to-noise in the C II and O II RLs and [Fe III] is too low to say conclusively what the morphology of the tail is in these species. The extinction map shown in Fig. 3 is not smooth on a spaxel to spaxel basis and shows local maxima along the ridge of [S II] emission noted above and at the position of the proplyd core.

It is challenging to produce a complete VLT optical spectrum throughout the range covered by the six Giraffe gratings taking into account that the LR1, 2, 3 set-ups were observed on a different night from the LR4, 5, 6 set-ups and over slightly different atmospheric conditions. It was therefore deemed appropriate to use the FOS 'M42-background' observations as a benchmark to which the Balmer decrement of the co-added LV 2 background spectrum observed by Argus (as defined above) was scaled. In this way the *mean* reddening obtained for the LV 2 background region is no longer a free parameter as it is equalized to 0.7 (from Table 2, third column). To achieve this, scaling factors of 1.070 and 0.833 were applied to the LR2 and LR6 spectra, respectively, while the LR1 spectrum was scaled to the LR2 spectrum using the H I λ3970 line common to both gratings. The LR3, 4, and 5 fluxes were left unscaled. The same scaling factors were then applied to the co-added LV 2 Core and Tail spectra whose reddening constants are considered to be free parameters.

4.1 Nebular reddening

Measured line fluxes and derived physical conditions are shown in Table 3 for the (*background-subtracted*) Core and Tail, as well as the Background spectra. The c(Hβ) reddening coefficients were derived from a comparison of the relative fluxes of the Hα, Hβ, Hγ, Hδ, and Hϵ lines with their theoretical values from Storey & Hummer (1995); Hα was saturated over the Core and so the line was not considered for this position. The Blagrave et al. (2007)–modified CCM law with $R_V = 5.5$ was used as previously. Resulting mean reddening constants are 1.20±0.08, 0.98±0.10 for the LV 2 Core and Tail regions (and 0.7 for the Background region). The c(Hβ) map computed from the Hγ/Hβ ratio if shown in Fig. 3. The reddening found from the Argus data over LV 2 Core is higher than the measurements by Blagrave et al. (2007) who found c(Hβ) = 0.82±0.04 from *HST* STIS data, but for a position ∼30 arcsec to the south-west. At the same time, the reddening derived by Blagrave et al. from FOS data is lower by 0.3 dex than from STIS for almost identical positions. Both STIS and Argus sampled a larger field of view than the FOS beam in each case and so the discrepancy may be due to line of sight reddening variations over areas larger than the 0.″26 FOS aperture. At a spatial resolution of 1.7 arcsec moderate values of c(Hβ) < 1 were found in the M42 Trapezium region by O'Dell & Yusef-Zadeh (2000). On the other hand, using high resolution speckle interferometry Schertl et al. (2003) found varying visual extinction of $A_V \sim$ (1.9, 3.8), (0.7, 7.8, >9.0), and 1.7 mag towards the resolved components of θ^1 Ori A, B, C respectively, or equivalently $c \sim$ (0.9, 1.8), (0.3, 3.6, >4.2), and 0.8; they also note that stronger extinction is correlated with the presence of circumstellar dust around the θ^1 Ori A2 and B3 companions.

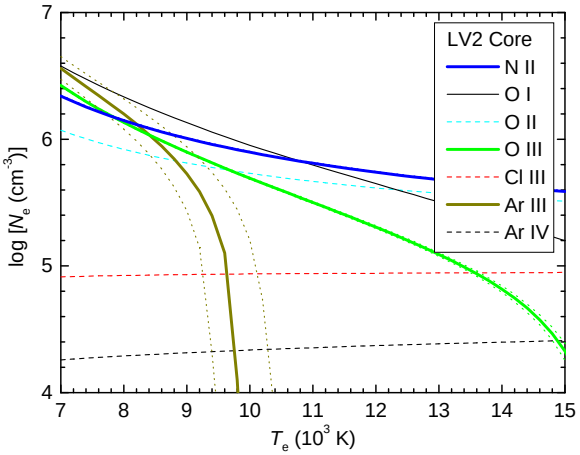

Figure 5. Electron temperature and density solutions for the background-subtracted core of LV 2 (as defined in the text). For [O III] and [Ar III] dotted lines bracketing thick solid lines correspond to min/max values of the diagnostic ratio. The O II curve is from the [O II] λ2470/(λ3726+λ3729) *HST* ratio.

In conclusion, while systematic effects on the absolute value of c(Hβ) are difficult to determine, the variations shown on the extinction map of Fig. 3 and the peaking of c(Hβ) over LV 2, associated with the VLT spectra, are suggestive of the presence of dust at that position. That the distribution of dust particles in M42 is variable over small spatial scales was shown by the mid-infrared mapping observations of Smith et al. (2005) at a diffraction-limited resolution of 0.″35. Viewed in the context of their figs 3 and 5, higher extinction values close to LV 2 could be justified as the proplyd and its immediate vicinity are a strong source of 11.7 μm continuum emission indicative of the presence of hot dust (100–150 K).

4.2 LV 2 electron temperatures and densities

Electron densities and temperatures from the Argus data were derived from various diagnostics. In Figs 5 and 6 a group of curves is shown on the (T_e, N_e) diagnostic plane representing solutions corresponding to the observed line ratios from Table 3. It should be noted that these ratios are for the rest velocity components of the lines in each case. For the Background region T_e = 9700±500 K is obtained for the singly ionized species and 8400±200 K for all other species with N_e = 4700±1400 cm^{-3}. For the Tail region T_e = 9700±300 K and log[N_e (cm^{-3})] = $4.58^{+0.24}_{-0.58}$ is adopted for all species. For the Core region, which is expected to be very dense, both the [O III] and especially the [N II] nebular to auroral ratios become more sensitive probes of N_e than they are of T_e; hence, the [N II] curve indicates $N_e > 6.7\times10^5$ cm^{-3} for T_e < 10 000 K and the intersection with the [O III] and [Ar III] λ5192/λ7135 curves yields (T_e, N_e) ≈ (8400 K, 1.1×10^6 cm^{-3}). At such high densities the usual optical diagnostic ratios – [O II] λ3726/λ3729, [S II] λ6716/λ6731, [Cl III] λ5518/λ5538, [Ar IV] λ4711/λ4740 – do not return

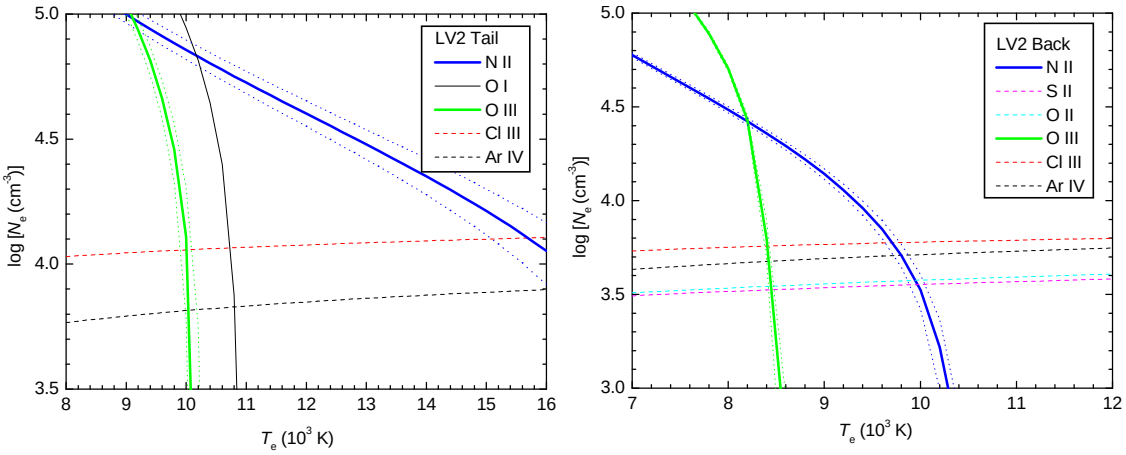

Figure 6. Electron temperature and density solutions for the (background-subtracted) tail and local background of LV 2. For [N II] and [O III] dotted lines bracketing thick solid lines correspond to min/max values of the diagnostic ratio.

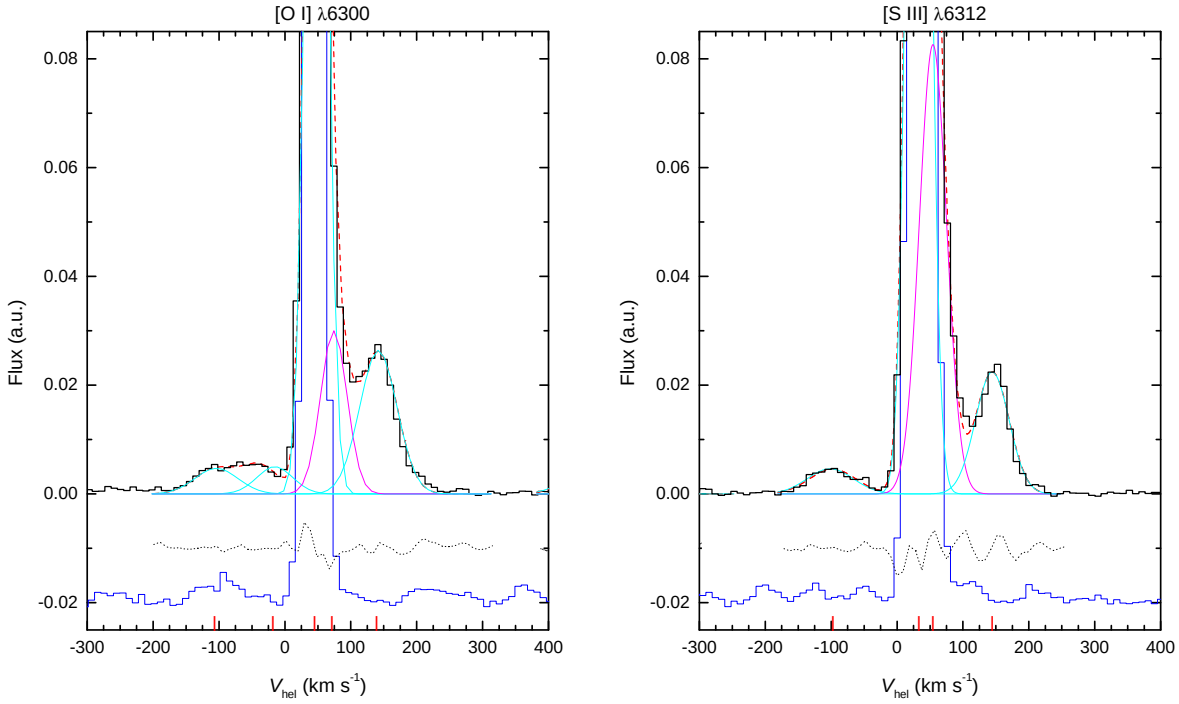

Figure 7. The velocity profiles of [O I] λ6300.34 Å and [S III] λ6312.10 Å at a resolution of 9.5 km s^{-1} per pixel from the VLT Argus spectrum (LR5 grating). Black: the LV 2 Core spectrum (observed minus the Background). Dashed red: multiple Gaussian fit to the Core spectrum – the individual velocity components are shown in cyan/magenta, the red vertical bars mark their centroids. The fit residuals are the dotted lines (shifted vertically by −0.01). Blue: The LV 2 Background spectrum as defined in the text (multiplied by a factor of 3.5, so that the rest velocity peak intensity of [O I] matches the one in the Core spectrum, and shifted vertically for clarity).

Table 3. Line fluxes and physical conditions of LV 2 from VLT FLAMES data.[a]

	Core	Tail	Background
$c(\mathrm{H}\beta)$	1.20±0.08	0.98±0.10	0.70±0.03
$F(\mathrm{H}\beta)$	$(1.570\pm0.001)\times10^{-13}$	$(1.820\pm0.001)\times10^{-14}$	$(7.440\pm0.001)\times10^{-14}$
		$I(\lambda)$	
[O II] λ3726	9.46 :	53.0±2.0	48.2±0.6
[Ne III] λ3868	45.0±1.2	30.7±1.6	21.7±0.4
[S II] λ4069	2.20±0.10	2.90±0.08	1.12±0.01
He I λ4471	4.22±0.10	4.14±0.10	5.04±0.10
[Fe III] λ4658	0.049±0.008	0.233±0.030	0.395±0.001
[Ar IV] λ4740	0.262±0.006	0.423±0.036	0.273±0.004
[O III] λ4959	119±0.4	111±0.6	123±0.1
[Ar III] λ5192	0.151±0.004	0.089±0.015	0.059±0.024
[Cl III] λ5539	0.089±0.005	0.399±0.025	0.548±0.003
He I λ5876	11.8±0.3	14.6±0.4	17.6±0.1
[O I] λ6300	1.54±0.05	1.33±0.06	0.751±0.010
[S III] λ6312	2.18±0.07	2.01±0.09	2.02±0.02
[N II] λ6584	7.94±0.33	39.1±2.0	32.0±0.5
He I λ6678	1.94±0.09	2.17±0.12	3.53±0.06
[S II] λ6731	0.256±0.011	2.92±0.16	2.89±0.04
C II λ4267	0.223 ±0.010	0.237±0.036	0.218±0.005
O II λ4638	0.042 ±0.007	–	0.055±0.003
O II λ4641	0.112 ±0.008	–	0.113±0.004
O II λ4649	0.154 ±0.007	0.172±0.027	0.163±0.004
O II λ4650	0.049 ±0.007	–	0.031±0.006
O II λ4661	0.043 ±0.008	–	0.052±0.003
O II λ4676	0.017 ±0.006	–	0.037±0.004
		$I(\lambda)$ ratios	
[O III] λ4959/λ4363	16.4±0.2	50.7±1.6	98.4±0.7
[O I] λ6300/λ5577	23.3±1.4	63.1:	–
[N II] λ6584/λ5755	2.78±0.02	21.1±1.3	61.2 ±1.2
[S II] λ6731/λ6716	2.64±0.01	2.35±0.04	1.66±0.004
[O II] λ3726/λ3729	2.50:	2.88±0.08	1.91±0.003
[Cl III] λ5539/λ5518	3.87±0.02	2.02±0.27	1.52±0.02
[Ar IV] λ4740/λ4711	2.30±0.02	1.26±0.18	1.15±0.03
		N_e (cm^{-3})	
[O I]	$1.4^{+0.1}_{-0.2}\times10^6$	–	–
[S II]	$\gtrsim10^4$	$\gtrsim10^4$	3400±200
[O II]	13300:	$\gtrsim10^4$	3500±200
[Cl III]	$8.3^{+0.3}_{-0.3}\times10^4$	$1.1^{+0.4}_{-0.3}\times10^4$	5800±900
[Ar IV]	$2.1^{+0.1}_{-0.1}\times10^4$	6500±2000	4800±1000
[N II]	$1.0^{+0.2}_{-0.1}\times10^6$	$8.0^{+0.1}_{-0.1}\times10^4$	–
		T_e (K)	
[O III]	9000±600	9700±300	8400±200
[N II]	–	–	9700±500

[a] $F(\mathrm{H}\beta)$ denotes observed fluxes in $\mathrm{erg\,cm^{-2}\,s^{-1}}$ per $0.31''\times0.31''$ spaxel; $I(\lambda)$ denotes dereddened relative intensities in units of Hβ = 100. The Core and Tail values refer to background-subtracted spectra. All entries are for the rest velocity components of the lines. Entries referring to [O II] λλ3726, 3729 in the Core spectrum are uncertain as the peak of LV 2 was very close to the edge of the field of view at this wavelength. ':' denotes very uncertain value.

reliable measurements as both their constituent lines are equally affected by collisional de-excitation. Here for the Core we adopt representative values of $T_\mathrm{e} = 9000 \pm 600$ K and $\log[N_\mathrm{e}\ (\mathrm{cm}^{-3})] = 5.90^{+0.10}_{-0.14}$ for all ions for which abundances are derived in Section 5. The upper density limit is consistent with the C III] λ1907/λ1909 ratio observations by Henney et al. (2002).

Additional evidence for the existence of high density ionized gas associated with LV 2 is given by the analysis of several [Fe III] $3d^6$ lines detected in the LR3 set-up. The rest velocity components of these lines are weak in the Core spectrum of LV 2 (only the strongest line in the multiplet λ4658.10 is detected along with λ4881), but their redshifted counterparts arising in gas outflowing from the Core are well-detected. This indicates that the abundance of iron must be enhanced in the redshifted outflow with respect to the Core and to the mean M42 value. An intensity-weighted mean of nine lines yields a heliocentric velocity of +155 ± 3 km s^{-1} for their emitting region. The λλ4607.0, 4881.1, 4931.0, and 5011.3 redshifted components show intensity ratios, relative to [Fe III] λ4658.10, of 0.103, 0.075, 0.153 and 0.382 respectively; a comparison with the theoretical intensities of Keenan et al. (2001) yields densities of (1.0 to 3.8)$\times10^6$ cm^{-3}. The above lines return unique solutions

to the density. Several more lines are detected ($\lambda\lambda$4701.62, 4733.90, 4769.40, 4777.70 Å) which provide both low and high solutions to the density. In all these cases, however, the high density solution is (2 to 4)$\times10^6$ cm^{-3} in agreement with the unique values found above. Arguably, if the outflow is this dense then the zero velocity ionized component at LV 2 could be denser.

Thus both the diagnostic ratio diagrams and the [Fe III] lines indicate that the ionized gas in the Core of LV 2 and in the proplyd redshifted outflow is of high density. An independent confirmation of our analysis is provided by Henney et al. (2002) who derived $N_e = 10^6$ cm^{-3} for the bright cusp of the proplyd from the C III] λ1907/λ1909 *HST* STIS ratio. (The individual C III] doublet components are not resolved in the FOS spectrum of Fig. 2).

A measurement of the neutral gas density in LV 2 is possible using the [O I] λ6300/λ5577 ratio which is sensitive to densities up to $\sim10^8$ cm^{-3}. The λ6300.34 line shows several velocity components in the Argus LR5 grating spectrum of the Core. A multiple Gaussian fit to the line profile is shown in Fig 7. Up to five components can be fitted. Two redshifted components are seen, each at a flux level of about 20 per cent with respect to the rest velocity component (Table 4). The blueshifted components have a total flux of 9 per cent with respect to the rest velocity. In the Background spectrum only the 0 km s^{-1} component is seen, and hence we conclude that the negative and positive velocity counterparts to the line are associated with LV 2 and arise from neutral gas present in the bipolar jet of the proplyd.

The [O I] λ5577 line in the LR4 grating shows only the two redshifted components at $V_\odot = +62.7 \pm 1.6$ and $+101 \pm 1$ km s^{-1} with a total flux of 20 percent with respect to the rest component; these are again absent from the Background. We thus took two [O I] λ6300/λ5577 ratios using first just the summed flux of the redshifted components and then the rest velocity components: these are 37.2 and 23.3 respectively (dereddened). At 8400 K they return N_e's of 9.5×10^5 and 1.8 $\times10^6$ cm^{-3} for the redshifted jet and the Core of LV 2 respectively. These results show that there is a reservoir of dense neutral gas in the proplyd which is being photoevaporated from it becoming entrained in a bipolar outflow. [2] This direct measurement of the density in the partly neutral outflow of LV 2 has repercussions for the mass-loss rate from the proplyd.

The fact that very high *electron* densities are probed via a neutral gas proxy (the [O I] ratio) leads to the conclusion that the emitting O^0 volume itself is substantially ionized (while at the same time the density of the inner neutral core of LV 2 must be even larger depending on its temperature). This is supported by the fact that emission from the highly ionized species [S III] is seen at similar velocities. An examination of the [S III] λ6312.10 line shows that it has one blueshifted and two redshifted velocity components present only in the LV 2 Core spectrum (Fig. 7 and Table 4). Depending on the exact geometry of the outflow this picture would suggest that the gas escaping from LV 2 becomes almost instantly ionized.

[2] A measurement of the density using [O I] in the Background spectrum is not possible as the λ5577 line is abnormally strong compared to published values for M42 from Esteban et al. (2004) – this indicates that the line suffers from telluric contamination: the Core and Tail spectra are immune to this as they are background-subtracted.

Table 4. The [O I] 6300.34, [S III] 6312.10, and [Fe III] 4658.10 Å line structure in the intrinsic LV 2 spectrum.[a]

$V_\odot$ (km s^{-1})	FWHM (km s^{-1})	Relative flux
	[O I]	
−107±12	71.6±18.9	0.05±0.01
−39.3±8.9	57.7±13.9	0.04±0.01
44.9±0.3	18.5±1.1	1.00±0.06
71.1±7.7	38.0±10.4	0.18±0.06
139±1	60.6±2.7	0.22±0.02
	[S III]	
−97.7±6.2	77.8±15.0	0.04±0.01
33.0±0.4	21.1±1.6	1.00±0.15
54.4±7.5	40.0±5.7	0.43±0.16
144±1	53.5±3.2	0.14±0.02
	[Fe III]	
−97.1±1.9	54.0±4.9	3.30±0.76
31.7±1.9	<16.7	1.00±0.20
155±1	35.9±1.3	11.1±2.3

[a] Velocities are heliocentric. The FWHMs have been corrected for instrumental broadening which for the LR5 grating is 28±1 km s^{-1} from Th-Ar arc line measurements. Fluxes are relative to the rest velocity component.

5 CHEMICAL ABUNDANCES

In this Section elemental abundances in LV 2 are derived using the direct measurements for the (T_e, N_e) obtained above. In Table 5 ionic abundances relative to H^+ are listed for the Core, Tail and Background regions of LV 2 based on CELs from the Argus data. The Core and Tail regions correspond to background-subtracted spectra and so these measurements should reflect more accurately the intrinsic composition of the proplyd.

Abundances were also computed from the Core, Tail and M42 filament FOS observations. For the Core, background-subtracted line intensities were used in order to be free from nebular contamination (see last column of Table 2). In this case the Tail FOS spectrum was adopted as background due to the 1″ proximity of the respective FOS pointings. The two M42 filament observations were not considered to be suitable for this purpose as they are 55 arcsec away and the Orion Nebula surface brightness varies considerably over such scales.

As the precise density stratification of LV 2 is unknown ionic abundances can be sensitive to the choice of N_e for their respective emitting zones if one relies only on lines of low N_{cr}; lines of high N_{cr} need to be considered for consistency otherwise some ionic ratios could be underestimated (Rubin 1989). In the determination of the O^+/H^+, O^{2+}/H^+, N^+/H^+, and S^+/H^+ ratios we also computed abundances from the λ2470, λ4363, λ5755, and λ4069 lines respectively (all with $N_{cr} > 10^6$ cm^{-3}). For instance, we found that regarding O^{2+}, at 9000 K and $\log[N_e(\mathrm{cm}^{-3})] = 5.9$, the difference in the ionic ratios from the λ5007 and λ4363 lines is 10 per cent. For N^+ the difference between abundances derived from the λ6584 and λ5755 lines is 30 per cent. For O^+ the λ3727 doublet returns a higher abundance ratio by 50 per cent compared to the λ2470 line. In such cases the

Table 5. Ionic abundances in LV 2 and its M42 vicinity (in a scale where log H = 12). The employed metallic lines were CELs but RL abundances are also listed for C^{2+} and O^{2+}.

	Core[a] VLT	Tail[b] VLT	Background[c] VLT	Core[d] FOS	Tail[e] FOS	M42[f] FOS
C^+	–	–	–	8.40±0.17	6.35±0.11:	8.17±0.17
C^{2+}	–	–	–	8.84±0.19	–	8.02±0.19
C^{2+} (RL)	8.32±0.05	8.35±0.05	8.32±0.05	–	–	–
N^+	7.44±0.14	7.17±0.10	6.91±0.10	7.68±0.14	7.29±0.10	7.66±0.05
O^+	–	8.30±0.23	7.90±0.17	8.75±0.18	7.90±0.09	8.53±0.07
O^{2+}	8.63±0.14	8.13±0.06	8.38±0.04	8.71±0.15	8.32±0.10	8.08±0.04
O^{2+} (RL)	8.54±0.10	8.54±0.10	8.57±0.10	–	–	–
Ne^{2+}	7.94±0.12	7.58±0.05	7.72±0.05	7.96±0.12	7.74±0.12	7.38±0.06
S^+	5.73±0.12	5.75±0.13	5.37±0.12	–	5.51±0.08	6.15±0.12
S^{2+}	6.77±0.10	6.67±0.03	7.03±0.05	6.63±0.11	7.07±0.11	6.60±0.05
Cl^{2+}	5.18±0.16	4.83±0.11	5.07±0.05	–	–	–
Ar^{2+}	6.44±0.12	6.04±0.05	6.27±0.05	6.53±0.08	6.27±0.09	6.03±0.11
Ar^{3+}	5.30±0.14	5.05±0.05	5.17±0.05	–	–	–
Fe^{2+}	4.67±0.10	5.16±0.07	5.56±0.05	–	–	–

[a] The core spectrum is background subtracted. $T_e = 9000 \pm 600$ K and $\log[N_e\ (cm^{-3})] = 5.90^{+0.10}_{-0.14}$ was adopted for all ions.

[b] The tail spectrum is background subtracted. Adopted $T_e = 9700 \pm 300$ K and $\log[N_e\ (cm^{-3})] = 4.58^{+0.24}_{-0.58}$.

[c] Adopted $T_e = 8400 \pm 200$ K for all non-singly ionized species and 9700 ± 500 K for singly ionized species with $N_e = 4700 \pm 1400$ cm^{-3}.

[d] The core spectrum is background subtracted. Adopted $T_e = 9050 \pm 650$ K with $\log[N_e\ (cm^{-3})] = 5.92^{+0.08}_{-0.10}$. The entries for the C^{2+} and O^{2+} RL abundances correspond to those of Core (VLT) as the FOS observation is spatially contained within the Core (VLT) observation.

[e] Adopted $T_e = 8950^{+1550}_{-1250}$ K with $\log[N_e\ (cm^{-3})] = 4.00^{+0.90}_{-0.32}$. The C^+ entry is very uncertain as it was obtained from a tentative C II] λ2326 detection.

[f] Adopted $T_e = 8850 \pm 250$ K with $\log[N_e\ (cm^{-3})] = 4.61^{+0.20}_{-0.38}$.

Table 6. The helium abundance in LV 2 and M42 vicinity.[a]

	Core FOS	Tail VLT	Background VLT	M42 filament FOS
He^+ (λ4471)	0.086 ±0.018	0.078 ±0.015	0.097 ±0.015	0.071±0.016
He^+ (λ5876)	0.094 ±0.009	0.095 ±0.010	0.118 ±0.011	0.071±0.011
He^+ (λ6678)	0.102 ±0.038	0.053 ±0.035	0.086 ±0.029	0.078±0.042
He^+/H^+ avg.	0.094 ±0.014	0.083 ±0.010	0.108 ±0.010	0.073±0.015
He/H	0.104±0.018	0.088±0.012	0.151 ±0.039	0.094±0.026

[a] The core and tail values are from background-subtracted spectra. Individual values were given weights of 1:3:1 in the computation of the mean according to the relative line intensities. The total He/H ratios incorporate corrections for the presence of neutral helium (Eq. 2).

mean was taken. For S^+ the value computed from the λ4069 line was adopted (from the VLT data as the line is blended with O II 3p–3d lines in the lower spectral resolution FOS spectrum).

Abundances for O^{2+} and C^{2+} were further computed from their respective O II and C II RLs detected in the three co-added VLT spectra and are included in Table 5. The following expression yields recombination line abundances relative to H^+:

$$\frac{X^{i+1}}{H^+} = \frac{\lambda}{4861.33}\ \frac{\alpha_{\rm eff}(H\beta)}{\alpha_{\rm eff}(\lambda)}\ \frac{I(\lambda)}{I(H\beta)}, \qquad (1)$$

where $I(\lambda)$ is the intensity at wavelength λ (Å) of an RL of the recombining ion X^{i+1}, and $\alpha_{\rm eff}(\lambda)$, $\alpha_{\rm eff}(H\beta)$ are the effective recombination coefficients for the line in question and Hβ, respectively. Recombination coefficients for O II and C II were taken from Storey (1994) and Davey et al. (2000), respectively. The He^+/H^+ ratio was obtained from the He I λ4471, λ5876, λ6678 RLs (Table 6), using effective recombination coefficients from Smits (1996) and correcting for the effects of collisional excitation using the formulae in Benjamin, Skillman & Smits (1999). A correction for the presence of neutral helium was estimated following Peimbert, Torres-Peimbert & Ruiz (1992) so that:

$$He/H = He^+/H^+ \times \left(1 + \frac{S^+}{S - S^+}\right). \qquad (2)$$

An estimate of the abundances of elements heavier than He can be made via ionization correction factor (ICF) methods based on standard schemes from the literature. The results are listed in Table 7 for the Core, Tail and local Background of LV 2 (helium abundances with and without cor-

Table 7. Total gas-phase abundances for the background-subtracted core and tail of LV 2, the local background, and a M42 filament (adopting $t^2 = 0$). Independent values for M42 (gas-phase) and the solar photosphere are listed (in units where $\log \mathrm{H} = 12$).

Element	LV 2 Core [1]	LV 2 Tail [1]	LV 2 Background [1]	Filament [1]	M42 ($t^2 = 0$) [2]	M42 ($t^2 = 0.022$) [2]	Sun [3]
He	10.973	10.919	11.033	10.863	–	10.942	10.93±0.01
He	11.017	10.944	11.179	10.973	10.991	10.988	–
C	8.98±0.15	–	(8.40±0.13)	8.40±0.13	–	–	8.43±0.05
C (RL)	8.66±0.10	8.35±0.11:	8.55±0.08	–	8.42±0.02	8.42±0.02	–
N	7.86±0.17	7.43±0.12	7.46±0.15	7.79±0.13	7.65±0.09	7.73±0.09	7.83±0.05
O	9.03±0.13	8.53±0.15	8.51±0.05	8.66±0.08	8.51±0.03	8.67±0.04	8.69±0.05
O (RL)	8.96±0.10	8.74±0.10	8.65±0.05	–	8.63±0.03	8.65±0.03	–
Ne	8.28±0.06	7.93±0.15	7.86±0.07	7.97±0.10	7.78±0.07	8.05±0.07	7.93±0.10
S	6.83±0.25	6.74±0.25	7.04±0.13	6.80±0.15	7.06±0.04	7.22±0.04	7.12±0.03
Cl	5.36±0.15	5.00±0.05	5.25±0.04	–	5.33±0.04	5.46±0.04	5.50±0.30
Ar	6.59±0.05	6.21±0.09	6.43±0.05	–	6.50±0.05	6.62±0.05	6.40±0.13
Fe	4.96±0.20	5.38±0.10	6.03±0.05	–	5.86±0.10	5.99±0.10	7.50±0.04

[a] The He entries are before and after including corrections for neutral helium respectively. The ICF scheme discussed in the text was used. For the Core the abundances from FOS were used for carbon and oxygen and the mean of VLT and FOS values were taken for nitrogen and neon; the other values were adopted from the VLT data. For the Tail and Background the VLT values were adopted; the carbon abundance for the Background was adopted from the M42 filament FOS position and may not be strictly representative of the local LV 2 background. References: [1] This work; [2] Esteban et al. (2004) for two values of the temperature fluctuation parameter, t^2 (e.g. Peimbert & Costero 1969); [3] Asplund et al. (2009).

rection for He^0 are included). Corrections for the unobserved ions N^{2+}, Ne^+, S^{3+} and Fe^+ were made as follows:

$$\mathrm{N/H} = \mathrm{N^+/H^+} \times (\mathrm{O^+ + O^{2+}})/\mathrm{O^+}, \quad (3)$$

$$\mathrm{Ne/H} = \mathrm{Ne^{2+}/H^+} \times (\mathrm{O^+ + O^{2+}})/\mathrm{O^{2+}}, \quad (4)$$

$$\mathrm{S/H} = (\mathrm{S^+ + S^{2+}})/\mathrm{H^+} \times \left[1 - (\frac{\mathrm{O^+}}{\mathrm{O^+ + O^{2+}}})^3\right]^{-1/3}, \quad (5)$$

$$\mathrm{Fe/H} = 0.9 \times (\mathrm{O^+/O^{2+}})^{0.08} \times (\mathrm{O/O^+}) \times \mathrm{Fe^{2+}/H^+}, \quad (6)$$

following Kingsburgh & Barlow (1994), Peimbert & Costero (1969), Stasinska (1978), and Rodríguez & Rubin (2005), respectively. The abundance of oxygen is the sum of O^+/H^+ and O^{2+}/H^+ ratios, and the abundance of carbon is the sum of C^+/H^+ and C^{2+}/H^+. For the determination of oxygen and carbon recombination line abundances we relied on the O II and C II RLs to obtain O^{2+}/H^+ and C^{2+}/H^+, but added in the O^+/H^+ and C^+/H^+ CEL values in each case (in the absence of O I and C I RLs). No UV carbon lines are detected by FOS from the Tail region (the C II] λ2326 detection is tentative) and so in estimating the carbon abundance using solely the C II λ4267 recombination line we corrected for the presence of C^+ adopting $\mathrm{ICF(C)} = \mathrm{O/O^{2+}}$ (Kingsburgh & Barlow 1994). Finally, in the cases of chlorine and argon we corrected for the presence of Cl^+ and Ar^+ adopting ICFs of 1.50±0.08 and 1.33±0.19, respectively, from the Orion Nebula study of Esteban et al. (2004). In Fig. 8 the various abundance measurements for the species considered in this analysis (except helium) are plotted.

5.1 Metallic recombination lines and the abundance anomaly

Recombination lines due to O II 3s–3p and C II 4f–3d transitions have been recorded by VLT Argus arising from LV 2 providing a measure of the O^{2+}/H^+ and C^{2+}/H^+ abundance ratios independently of the [O III] and C III] CELs. The lines have previously been detected in Herbig-Haro objects in M42 (Blagrave et al. 2006; Mesa-Delgado et al. 2009), as well as in the diffuse M42 gas (e.g. Esteban et al. 2004). Here, several O II V1 multiplet lines near 4650 Å are detected along with C II λ4267.15 which is the strongest metallic RL accessible in the optical (Fig. 9). Intensity maps of O II λ4649 and C II λ4267 are shown in Fig. 3. The lines are intrinsically faint with intensities of less than one per cent of $I(\mathrm{H}\beta)$ but offer the advantage that the ratio of their emissivities to H I lines is a weak function of the plasma temperature and density (Storey 1994; Storey & Hummer 1995; Liu et al 1995; Davey et al. 2000; Tsamis et al. 2004). The derived abundances should thus be less prone to errors resulting from uncertainties in the measurement of these quantities (e.g. Peimbert et al. 1993; Tsamis et al 2003a; Esteban et al 2004). This is in contrast to abundances derived from ratios of CELs to H I lines which have an exponential sensitivity to the electron temperature, and also depend on N_e when CELs of low N_cr are used (e.g. Rubin 1989; Tsamis et al. 2003b).

The well-documented abundance anomaly in H II regions refers to the fact that higher abundances of O^{2+}/H^+ and C^{2+}/H^+ are derived from O II and C II RLs than from the [O III] and C III] CELs of the same ions (e.g. Peimbert et al. 1993; Tsamis et al. 2003a; Mesa-Delgado & Esteban 2010). This has repercussions for the representative abundances of O/H and C/H in the nebulae and by extension for the metallicity of the galaxies that host them. The ratio of RL to CEL abundance determinations for a given ion (the so-called abundance discrepancy factor, ADF) takes values from ∼2 to 5 in H II regions, and is best measured for O^{2+} which has RLs (e.g. 4649.13 Å) and CELs (e.g. 4958.91, 5006.84 Å) falling in the blue part of the spectrum that can be observed simultaneously with the same telescope/spectrograph configuration. It is more difficult to obtain the ADF for C^{2+} which has a CEL in the UV (the C III] 1908 Å intercombination doublet) and a RL in the blue (C II 4267 Å) and be certain that the same volume

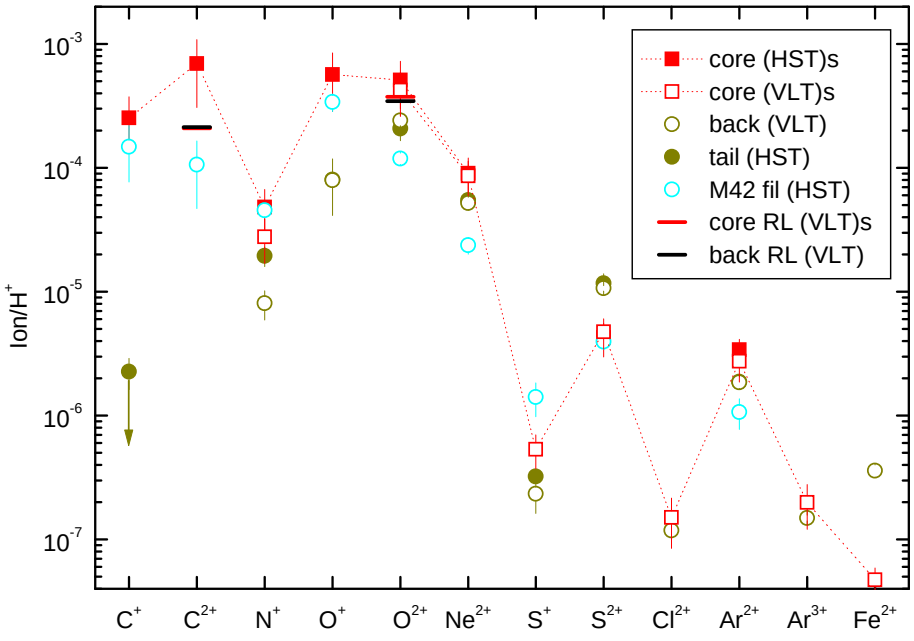

Figure 8. Ionic gas phase abundances in LV 2 and in its Orion Nebula vicinity from the present analysis. Abundances were computed from collisionally excited lines. For C^{2+} and O^{2+} abundances from recombination lines are shown as horizontal bars. In the key box 's' refers to values from background subtracted spectra.

of nebula is sampled as data obtained from different telescopes/apertures need to be combined.

We take advantage of the co-spatial coverage over LV 2 of C III] λ1908 and C II λ4267 with FOS and Argus respectively to measure both the C^{2+} and O^{2+} ADFs with a good degree of confidence. In Table 8 the values that we obtained are listed for the LV 2 Core, Tail and Tip positions and for the local nebula background in the form of

$$\mathrm{ADF}(\mathrm{X}^{2+}) \equiv \frac{(\mathrm{X}^{2+}/\mathrm{H}^{+})_{\mathrm{RL}}}{(\mathrm{X}^{2+}/\mathrm{H}^{+})_{\mathrm{CEL}}}. \qquad (7)$$

The quoted uncertainties are not due to formal errors but are associated with the variation of the quantity arising from the range of the CEL-computed abundances (with their known sensitivity to $T_{\rm e}$ and $N_{\rm e}$). Values are tabulated for the background-subtracted spectra but also for the observed spectra which include the M42 nebular emission, so as to examine the difference in the numbers obtained. The O^{2+}/H^{+} and C^{2+}/H^{+} RL ratios in Table 5 were derived from the VLT data. Additionally, the $12+\log(O^{2+}/H^{+})$ and $12+\log(C^{2+}/H^{+})$ RL ratios corresponding to the *observed* Core VLT spectrum are 8.65±0.05, 8.37±0.04, while those from the *observed* Tail VLT spectrum are 8.57±0.05 and 8.35±0.04 respectively. These along with the corresponding CEL values listed in the footnotes of Table 8 were used to obtain the ADFs corresponding to the intrinsic as well as the nebula-contaminated (observed) LV 2 spectra.

Table 8. Abundance discrepancy factors: the ratio of RL to CEL abundance determinations for O^{2+} and C^{2+}.[a]

	ADF(O^{2+})	ADF(C^{2+})
	Background-subtracted spectra	
Core (VLT)	$0.8^{+0.6}_{-0.3}$	–
Core (FOS)	$0.7^{+0.5}_{-0.3}$	$0.3^{+0.2}_{-0.1}$
Tail (VLT)	$2.6^{+1.1}_{-0.8}$	–
Tip (FOS)	$0.7^{+0.4}_{-0.3}$	$0.3^{+0.3}_{-0.1}$
	Observed spectra	
Core (VLT)	$1.9^{+3.1}_{-0.7}$	–
Core (FOS)	$2.1^{+2.5}_{-0.8}$	$1.2^{+3.2}_{-0.5}$
Tail (FOS)	$1.8^{+0.3}_{-0.3}$	–
Tip (FOS)	$3.3^{+1.0}_{-0.6}$	$3.9^{+2.2}_{-1.0}$
Background (VLT)	$1.5^{+0.6}_{-0.4}$	–

[a] The C^{2+}/H^{+} and O^{2+}/H^{+} RL ratios were obtained from the VLT spectra in all cases (Table 3). In units where $\log \mathrm{H} = 12$ the corresponding CEL abundance ratios used to compute the ADFs are: for the background-subtracted spectra of Core (VLT), Core (FOS), Tail (VLT) see Table 5; for Tip (FOS): $O^{2+} = 8.75$, $C^{2+} = 8.85$ (at $T_{\rm e} = 9000$ K, $\log[N_{\rm e}\ (\mathrm{cm}^{-3})] = 5.81$). For the observed spectra – Core (VLT): $O^{2+} = 8.38^{+0.21}_{-0.43}$ (at $T_{\rm e} = 9650\pm1350$ K, $\log[N_{\rm e}\ (\mathrm{cm}^{-3})] = 5.29^{+0.29}_{-1.48}$) ; Core (FOS): $O^{2+} = 8.33^{+0.19}_{-0.61}$, $C^{2+} = 8.29^{+0.24}_{-0.57}$ using data from Table 2; Tail (FOS) see Table 5; Tip (FOS): $O^{2+} = 8.13^{+0.08}_{-0.11}$, $C^{2+} = 7.79^{+0.13}_{-0.20}$ using data from Table 2; Background (VLT) see Table 5.

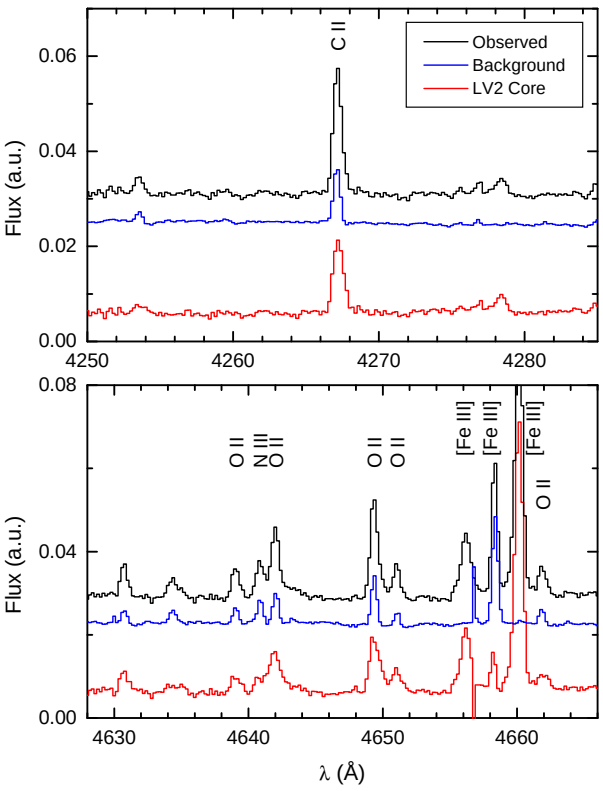

Figure 9. The C II 4267.15 Å $3d\,^2D - 4f\,^2F^o$ and O II V1 multiplet $3s\,^4P - 3p\,^4D^o$ recombination lines on the VLT Argus spectrum of LV 2 at a resolution of 9.5 km s^{-1} per pixel. Black: Observed (proplyd + M42 nebula), Blue: local M42 nebula background, and Red: LV 2 Core (observed minus the background). Note the blue- and red-shifted components of [Fe III] 4658 Å which arise in the outflow.

6 DISCUSSION AND CONCLUSIONS

The gas-phase abundances of light metals in LV 2 measured via UV and optical emission line spectroscopy are generally higher than those in the Orion Nebula. The differences are the largest for carbon and oxygen when comparing values obtained from CELs. The differences become smaller when the recombination line results are compared: $\Delta C = +0.11$ and $\Delta O = +0.31$ dex. Assuming that the RL values for these two elements are more reliable then LV 2 has a carbon abundance a factor of 1.3–1.7 higher than M42 (when comparing with the local background or with Esteban et al. 2004), and a factor of 1.7 higher than the solar value by Asplund et al. (2009). If some of the C is locked in grains, particularly in the inner disk regions, then the difference with the sun would be even higher. For nitrogen there are no substantial differences between LV 2, M42 (for $t^2 = 0.022$) or the sun. The oxygen abundance in LV 2 is higher by a factor of ∼2 compared to the local background, M42, or the sun. Again the difference with the sun would be greater if the unknown amount of oxygen incorporated in solids was considered. Neon, which as a noble gas is not expected to be affected by depletion on grains, is also overabundant by a factor of 2.2–2.6 compared to the sun and the local nebula, or a factor or 1.9 when comparing with the recent determination in M42 of 8.01±0.01, based on *Spitzer* data (Rubin et al. 2010). The solar Ne abundance is however controversial as Drake & Testa (2005) have advocated a value ∼2.5 times higher than Asplund et al. (2009); this would bring the LV 2 and solar neon abundances into agreement.

The oxygen and neon abundances in LV 2 are consistent with the range of abundances in the X-ray bright coronae of 35 pre-main sequence Orion Nebula Cluster stars observed by Maggio et al. (2007); the oxygen abundance is ≈0.2 dex higher than in 13 early B-type stars of the Ori OB1 association studied by Simon-Diaz (2010).

The sulphur abundance is consistent with the M42 value within the uncertainties. Chlorine too is consistent with the M42 value, and the sun. The argon abundance is in agreement with that in B-type stars of the Orion association (6.66±0.06; Lanz et al. 2008), and in M42. The iron abundance is most certainly severely underestimated as the important Fe^+ ion is not observed, and a large percentage of the total must be in the dust phase; the same is true for the local nebula as the expected dominant Fe^{3+} ion (e.g. Rubin et al. 1991) is not observed here. As a result, the iron abundance estimates for LV 2 and M42 cannot be directly compared with the sun.

The second noteworthy result from this study is that the abundance anomaly, classically manifested by $ADF(X^{+i}) > 1.0$, goes away when one considers the intrinsic spectrum of the proplyd, that is, with the foreground/background nebula contamination removed (Table 8)[3]. The upward correction overwhelmingly affects the temperature and density dependent CEL diagnostics, not the RLs. In this case the RL and CEL abundances for oxygen come into very good agreement for the Core and Tip regions of LV 2, which encompass a large part of the luminous flux from the object. The carbon abundance derived from the UV CELs is then a factor of 2–3 higher that the RL value. This however could be due to an underestimation of the T_e in the zone emitting the 1908 Å line, the most temperature sensitive line in this study; adopting a value in the upper T_e range (∼9700 K) the CEL and RL measurements would come into agreement.

These effects on the ADF are due to the disproportionate bias that the H II region contamination imparts on the CEL temperature and abundance diagnostics compared to the RL diagnostics: the $I_{sumV1}(O\ II)/I(H\beta)$ and $I(C\ II\ \lambda4267)/I(H\beta)$ intensity ratios are practically the same in the intrinsic LV 2 core spectrum and in the LV 2 core + M42 spectrum. In this sense the proplyd is not a prolific metallic RL emitter such as the inner regions of planetary nebulae (e.g. Tsamis et al. 2008). However considering the high emission measure ($\int N_e\ N_H\ dV$) of the skin-deep but very dense photoionized layer of the proplyd one could instead say that LV 2 is at least as prolific a C II, O II RL emitter as the diffuse Orion Nebula along the same line of sight. At the same time, the proplyd appears hotter, less

[3] With the exception of the Tail region where the background subtraction was probably not as accurate due to its extended nature.

dense and with a lower (forbidden-line) oxygen and carbon abundance when the M42 contribution to the relevant CELs is neglected than when this contribution is subtracted.

If one considers that the decades old ADF problem has been solved in the case of LV 2 'simply' by subtracting the H II region spectrum and examining in detail the spectrum of one dense clump where the margin of uncertainty in the derived quantities is reduced, then one is impelled to acknowledge the following:

(i) In the presence of a population of small and dense partially-ionized clumps along a random line of sight, the CEL-derived Orion Nebula gaseous abundances would be lower limits based on the principles discussed above (cf. also Rubin 1989; Viegas & Clegg 1994). In the vicinity of LV 2 the gas-phase M42 abundances would in fact lie somewhere between the LV 2 Core and local background values.

(ii) The simplest solution to the so-called ADF/t^2 problem encountered in H II regions would then be one where density inhomogeneities are playing havoc with the classic forbidden line diagnostics.

(iii) The metallicity of nebulae where spatially resolved observations are impossible, such as extragalactic H II regions, will need to be corrected upwards. Whether there will be repercussions for cosmic chemical evolution studies will depend on the correction factor and how that factor varies with metallicity or other properties of the ionized interstellar medium, such as the degree of 'clumpiness'.

ACKNOWLEDGMENTS

We wish to thank the FLAMES support astronomers at ESO for scheduling the VLT service mode observations. Thanks also to Bob Rubin, Bob O'Dell, and the referee for helpful comments. This research has used *HST* data obtained from the Space Telescope European Coordinating Facility's archive at ESO. YGT and JMV acknowledge funding from grants AYA2007-67965-C03-02/CSD2006-00070 (Ingenio-Consolider 2010) of the Spanish Ministry of Science and Innovation.

YGT further acknowledges the award of a Marie Curie intra-European Fellowship within the 7$^{\rm th}$ European Community Framework Programme (grant agreement PIEF-GA-2009-236486).

REFERENCES

Asplund, M., Grevesse, N., Jacques Sauval, A., & Scott, P. 2009, ARA&A, 47, 481
Bally, J., O'Dell, C. R., & McCaughrean, M. J. 2000, AJ, 119, 2919
Benjamin, R. A., Skillman, E. D., & Smits, D. P. 1999, ApJ, 514, 307
Blagrave, K. P. M., Martin, P. G., & Baldwin, J. A. 2006, ApJ, 644, 1006
Blagrave, K. P. M., Martin, P. G., Rubin, R. H., Dufour, R. J., Baldwin, J. A., Hester, J. J., & Walter, D. K. 2007, ApJ, 655, 299
Blecha, A., & Simond, G. 2004, GIRRAFE BLDR Software Reference Manual 1.12 (http://girbldrs.sourceforge.net)
Cardelli, J. A., Clayton, G. C., & Mathis, J. S. 1989, ApJ, 345, 245 (CCM)
Davey, A. R., Storey, P. J., & Kisielius, R. 2000, A&ASupplement, 142, 85
Doi, T., O'Dell, C. R., & Hartigan, P. 2004, AJ, 127, 3456
Drake, J. J., & Testa, P. 2005, Nature, 436, 525
Esteban, C., Peimbert, M., García-Rojas, J., Ruiz, M. T., Peimbert, A., & Rodríguez, M. 2004, MNRAS, 355, 229
Esteban, C., Bresolin, F., Peimbert, M., García-Rojas, J., Peimbert, A., & Mesa-Delgado, A. 2009, ApJ, 700, 654
Ercolano, B. 2009, MNRAS, 397, L69
García-Rojas, J., Esteban, C., Peimbert, M., Rodríguez, M., Ruiz, M. T., & Peimbert, A. 2004, ApJS, 153, 501
Gonzalez, G. 1997, MNRAS, 285, 403
Gonzalez, G., Laws, C., Tyagi, S., & Reddy, B. E. 2001, AJ, 121, 432
Henney, W. J., O'Dell, C. R., Meaburn, J., Garrington, S. T., & Lopez, J. A. 2002, ApJ, 566, 315
Johnstone, D., Hollenbach, D., & Bally, J. 1998, ApJ, 499, 758
Jones, B. F., & Walker, M. F. 1988, AJ, 95, 1755
Keenan, F. P., Aller, L. H., Ryans, R. S. I., & Hyung, S. 2001, Proceedings of the National Academy of Science, 98, 9476
Keyes, C. D., Koratkar, A. P., Dahlem, M., et al. 1995, Faint Object Spectrograph Instrument Handbook, 6th edition, STScI
Kingsburgh, R. L., & Barlow, M. J. 1994, MNRAS, 271, 257
Laws, C., Gonzalez, G., Walker, K. M., Tyagi, S., Dodsworth, J., Snider, K., & Suntzeff, N. B. 2003, AJ, 125, 2664
Lanz, T., Cunha, K., Holtzman, J., & Hubeny, I. 2008, ApJ, 678, 1342
Laques, P., & Vidal, J. L. 1979, A&A, 73, 97
Liu X.-W., Storey P. J., Barlow M. J., Clegg R. E. S., 1995, MNRAS, 272, 369
Maggio, A., Flaccomio, E., Favata, F., Micela, G., Sciortino, S., Feigelson, E. D., & Getman, K. V. 2007, ApJ, 660, 1462
McCaughrean, M. J., & O'dell, C. R. 1996, AJ, 111, 1977
Meaburn, J., Massey, R. M., Raga, A. C., & Clayton, C. A. 1993, MNRAS, 260, 625
Mesa-Delgado, A., Esteban, C., & García-Rojas, J. 2008, ApJ, 675, 389
Mesa-Delgado, A., Esteban, C., García-Rojas, J., Luridiana, V., Bautista, M., Rodríguez, M., López-Martín, L., & Peimbert, M. 2009, MNRAS, 395, 855
Mesa-Delgado, A., & Esteban, C. 2010, arXiv:1003.2567, MNRAS (in press)
Neves, V., Santos, N. C., Sousa, S. G., Correia, A. C. M., & Israelian, G. 2009, A&A, 497, 563
O'Dell, C. R., Wen, Z., & Hu, X. 1993, ApJ, 410, 696
O'Dell, C. R., & Wen, Z. 1994, ApJ, 436, 194
O'Dell, C. R., & Yusef-Zadeh, F. 2000, AJ, 120, 382
O'Dell, C. R., Peimbert, M., & Peimbert, A. 2003, AJ, 125, 2590
O'Dell, C. R., Muench, A., Smith, N., & Zapata, L. 2008, Handbook of Star Forming Regions, Volume I: The Northern Sky ASP Monograph Publications, Vol. 4. Edited by Bo Reipurth, p. 544
O'Dell, C. R., & Harris, J. A. 2010, arXiv:1008.1002, AJ accepted
Osterbrock, D. E. 1989, Astrophysics of gaseous nebulae and active galactic nuclei, Mill Valley, CA, University Science Books
Pasquini, L., et al. 2002, The Messenger 110, 1
Peimbert, M., & Costero, R. 1969, Boletin de los Observatorios Tonantzintla y Tacubaya, 5, 3
Peimbert, M., Torres-Peimbert, S., & Ruiz, M. T. 1992, Rev. Mex. Astron. Astrofis, 24, 155
Peimbert, M., Storey, P. J., & Torres-Peimbert, S. 1993, ApJ, 414, 626
Peimbert, A. 2003, ApJ, 584, 735
Reid, M. J., et al. 2009, ApJ, 700, 137
Rodríguez, M., & Rubin, R. H. 2005, ApJ, 626, 900
Rubin, R. H. 1989, ApJS, 69, 897
Rubin, R. H., Simpson, J. P., Haas, M. R., Erickson, E. F. 1991, PASP, 103, 834

Rubin, R. H., Martin, P. G., Dufour, R. J., Ferland, G. J., Blagrave, K. P. M., Liu, X.-W., Nguyen, J. F., & Baldwin, J. A. 2003, MNRAS, 340, 362
Rubin, R. H., Simpson, J. P., O'Dell, C. R., McNabb, I. A., Colgan, S. W. J., Zhuge, S. Y., Ferland, G. J., & Hidalgo, S. A. 2010, arXiv:1008.2736, MNRAS accepted
Santos, N. C., Israelian, G., & Mayor, M. 2000, A&A, 363, 228
Schertl, D., Balega, Y. Y., Preibisch, Th., Weigelt, G. 2003, A&A, 402, 267
Simón-Díaz, S. 2010, A&A, 510, A22
Smith, N., Bally, J., Shuping, R. Y., Morris, M., & Kassis, M. 2005, AJ, 130, 1763
Smits, D. P. 1996, MNRAS, 278, 683
Stasińska, G. 1978, A&A, 66, 257
Storey, P. J. 1994, A&A, 282, 999
Storey, P. J., & Hummer, D. G. 1995, MNRAS, 272, 41
Tsamis, Y. G., Barlow, M. J., Liu, X.-W., Danziger, I. J., & Storey, P. J. 2003a, MNRAS, 338, 687
Tsamis Y. G., Barlow M. J., Liu X.-W., Danziger I. J., Storey P. J., 2003b, MNRAS, 345, 186
Tsamis, Y. G., Barlow, M. J., Liu, X.-W., Storey, P. J., & Danziger, I. J. 2004, MNRAS, 353, 953
Tsamis, Y. G., & Péquignot, D. 2005, MNRAS, 364, 687
Tsamis, Y. G., Walsh, J. R., Péquignot, D., Barlow, M. J., Danziger, I. J., & Liu, X.-W. 2008, MNRAS, 386, 22
Tsamis, Y. G., Walsh, J. R., & Péquignot, D. 2009, Science with the VLT in the ELT Era, Astrophysics and Space Science Proceedings, 61
Vasconcelos, M. J., Cerqueira, A. H., Plana, H., Raga, A. C., & Morisset, C. 2005, AJ, 130, 1707
Viegas, S. M., & Clegg, R. E. S. 1994, MNRAS, 271, 993
Walsh, J. R., & Rosa, M. R. 1999, Chemical Evolution from Zero to High Redshift, Proceedings of the ESO Workshop held at Garching, edited by J.R. Walsh, M. R. Rosa, Berlin: Springer-Verlag, 68
Walsh, J. R., & Roy, J. R. 1990, 2nd ESO/ST-ECF Data Analysis Workshop, ESO Conference and Workshop Proceedings, edited by D. Baade and P.J. Grosbøl, 34, 95
Zeippen, C. J. 1982, MNRAS, 198, 111